Hydrogen peroxide-responsive AIE probe for imaging-guided organelle targeting and photodynamic cancer cell ablation

Qian Wu,[a,b] Youmei Li,[a,b] Ying Li,*[a] Dong Wang*[a] and Ben Zhong Tang *[c,d]

[a] Center for AIE Research, Shenzhen Key Laboratory of Polymer Science and Technology, Guangdong Research Center for Interfacial Engineering of Functional Materials, College of Materials Science and Engineering, Shenzhen University, Shenzhen 518061 (P. R. China). E-mail: wangd@szu.edu.cn.

[b] Key Laboratory of Optoelectronic Devices and Systems of Ministry of Education and Guangdong Province, College of Optoelectronic Engineering, Shenzhen University, Shenzhen, 518060, China.

[c] Department of Chemistry, Hong Kong Branch of Chinese National Engineering Research Center for Tissue Restoration and Reconstruction, The Hong Kong University of Science and Technology, Clear Water Bay, Kowloon, Hong Kong, 999077, China. E-mail: tangbenz@ust.hk.

[d] NSFC Center for Luminescence from Molecular Aggregates, SCUT-HKUST Joint Research Institute, State Key Laboratory of Luminescent Materials and Devices, South China University of Technology, Guangzhou 510640, China.

Abstract: Hydrogen peroxide (H_2O_2), as one kind of key reactive oxygen species (ROS), is mainly produced endogenously primarily in the mitochondria. The selective monitoring of H_2O_2 in living cells is of great significance for understanding diagnosis and pathogenesis of cancers, the Alzheimer's disease and diabetes. Here, we constructed a versatile AIE probe, TTPy-H_2O_2, which achieved superb performances in the specifically visualization of H_2O_2 specifically in various living cells with mitochondria targeting, excellent biocompatibility and photostability, and remarkable ROS generation ability. Red/near-infrared fluorescence firstly located in the mitochondria could light up lipid droplets with bright yellow fluorescence after responding to the H_2O_2, which can realize both imaging and photodynamic therapy (PDT) for cancer therapy.

1. Introduction

Reactive oxygen species (ROS), mainly including singlet oxygen ($^1O_2$), superoxide anion ($O_2^{\cdot-}$), hydrogen peroxide (H_2O_2), and hydroxyl radical (HO·), are produced endogenously as by-products of cellular metabolism primarily in the mitochondria, and serve as indispensable messengers involving in multiple physiological processes.[1-6] H_2O_2, as a kind of representative ROS, has received growing concern by the virtue of its oxidative damage of biomacromolecules such as proteins, liposomes and DNA when overproduced or excessively accumulated. Increasing evidence indicates that the unbalance of H_2O_2 homeostasis is related to various human diseases including cancers, the Alzheimer's disease, diabetes, and aging.[7-11] Specifically, it may estimate that there is much higher concentration of H_2O_2 in cancer cells (10-100 μM) than those in normal cells (0.001–0.7 μM).[12-14] As a consequence, it is of great significance to develop novel imaging methods which allow real-time monitoring of the level of H_2O_2 in the living cells, and provide instructive guidance for the diagnosis and further therapy of cancers.

In the past decades, fluorescence imaging has been regarded as one of the most promising imaging methods in living system on account of its distinctive advantages including non-invasiveness, high-sensitivity, and low-cost. A variety of organic fluorescence bioprobes have been designed and constructed for the selective detection of H_2O_2 in the living cells.[15-21] Thereinto, fluorogens with aggregation-induced emission (AIE) characteristics have arisen as a novel family of

fluorescence imaging materials and enjoyed omnipotent applications in bioimaging, biosensing and therapeutics.[22-24] They usually possess the unique superiorities of modifiable structure, large Stokes-shift, low background, and good stability against photobleaching, which endows them with great potentials in real-time monitoring of bioactive molecules like H_2O_2 in living system.[25-28]

To date, several works have been reported to implement a "turn-on" fluorescence by utilizing AIE bioprobe to selectively react with H_2O_2 and achieve aggregation-induced emission in cytoplasm or specific organelles.[29-32] Moreover, reasonable regulation of energy in the excited state enables AIE bioprobe to image H_2O_2 in living cells and simultaneously ablate cancer cells by photodynamic therapy (PDT) and photothermal therapy (PTT).[33,34] However, rare research has focus on the real-time monitoring of H_2O_2 and visualizing dynamic change of organelles, especially for the mitochondria, in the process of PDT.

In view of the above situation, here we designed and constructed a H_2O_2-responsive AIE probe for targeted organelle imaging and PDT of cancer cells for the first time. As shown in Scheme 1, a versatile fluorescent probe termed as TTPy-H_2O_2 was ingeniously designed on the basis of the following considerations. Firstly, *p*-pinacolborylbenzyl moiety was adopted as reaction unit on account of its unique reactivity with H_2O_2 which has been demonstrated in the previous work.[16,35] Then pyridinium cation was introduced to allow specifically targeting mitochondria by the electrostatic interaction with electronegative mitochondrial membrane.[36,37] More importantly, it was also utilized as strong electron acceptor and linked to triphenylamine-thiophene building block, constructing a twisted donor-acceptor (D-A) structure which will facilitate the red-shift of emission wavelength and large Stokes shift. Besides, the multiple freely rotatable phenyl groups and double bond were beneficial to quenching fluorescence in the solution while endowing strong aggregation-induced emission in the targeted organelles.[38,39] According to our preliminary study, this strong D-A structure showed great potential to be a good photosensitizer for PDT.[40-42] As expected, the AIE probe TTPy-H_2O_2 with red/near-infrared (NIR) emission and moderate water solubility firstly lighted up mitochondria specifically in living cells. After reacting with overproduced H_2O_2 primarily in the mitochondria of cancer cells, TTPy-H_2O_2 was transformed to be a yellow-emissive fluorogen, TTPy, which can be real-time monitored synchronously with TTPy-H_2O_2 in different channels of confocal laser scanning microscope (CLSM). Interestingly, hydrophobic TTPy was observed to easily transfer into lipid droplets (LD). Hence, our AIE probe TTPy-H_2O_2 with mitochondria targeting can make a selectively response to H_2O_2 in living cells. The synchronous changes of fluorescence wavelength and the organelle targeting can serve as an indicator for the further PDT on cancer cells. In addition, this H_2O_2 responsive and dual signals read-out can indicate the performance of PDT in living cells to demonstrate the efficient generation of singlet oxygen and effective ablation of cancer cells. The dynamic change of mitochondria in the process of PDT can be monitored in real-time, which provides a novel insight to investigate the damage mechanism of ROS in living system and the related diseases.

2. Experimental section

Materials and instruments

All the chemicals and biological reagents for synthesis and analysis were purchased from Energy, Bide and Sigma-Aldrich Chemical Reagent Ltd., and used without further purification unless specified requirement. Nuclear magnetic resonance (NMR) spectra were measured on Bruker AVANCE III 400MHZ and 500MHZ NMR spectrometers. High resolution mass spectrometer (HRMS) was tested on Thermo Exactive Focus Q. UV-vis absorption spectra were measured on a PerkinElmer Lambda 950 spectrophotometer. Fluorescence spectra were recorded on Edinburgh FS5 fluorescence spectrophotometer. Quantum yield was determined by a Quanta-integrating sphere. Fluorescence images were collected on a confocal laser scanning microscope (CLSM, ZEISS-LSM900) and analyzed by using ZEN 3.2 software. The 3-(4,5-dimethyl-2-thiazolyl)-2,5-diphenyl-2-*H*-tetrazolium bromide (MTT) assay was conducted on a BioTek microplate reader.

Synthesis of TTPy-H_2O_2

4-Bromomethylphenylboronic acid pinacol ester (150 mg, 0.5 mmol) and TTPy (215 mg, 0.5 mmol) were refluxed under nitrogen in dry acetonitrile (10 mL) at 80 ^oC for 8 h. After cooling to room temperature, the mixture was added into 50 mL of ice-cooled diethyl ether with vigorous stirring. The precipitates were separated by centrifugation and washed three times with diethyl ether and dried in a vacuum at 40 ^oC to a constant weight. Eventually, TTPy-H_2O_2 was obtained as deep red powder in 88% yield (320 mg). ^1H NMR (400 MHz, CD_2Cl_2) δ 9.08 (d, J = 6.6 Hz, 2H), 8.00 (d, J = 15.7 Hz, 1H), 7.92 (d, J = 6.6 Hz, 2H), 7.78 (d, J = 8.0 Hz, 2H), 7.56 (d, J = 8.1 Hz, 2H), 7.46 – 7.40 (m, 3H), 7.28 (dd, J = 8.8, 7.1 Hz, 4H), 7.17 (d, J = 3.9 Hz, 1H), 7.08 (d, J = 7.5 Hz, 6H), 6.99 (d, J = 8.8 Hz, 2H), 6.75 (d, J = 15.8 Hz, 1H), 6.05 (s, 2H), 1.30 (s, 12H). ^{13}C NMR (101 MHz, CD_2Cl_2) δ 154.06, 149.92, 149.09, 147.59, 144.37, 139.11, 136.84, 136.16, 135.88, 135.28, 129.97, 129.00, 127.34, 127.06, 125.61, 124.29, 124.07, 123.88, 122.94, 120.38, 84.61, 63.37, 25.19. HRMS: calcd. for $[C_{42}H_{40}BN_2O_2S]^+$: 647.2898, found 647.2922.

3. Results and discussion

Molecular synthesis of TTPy-H_2O_2

As shown in experimental section and supplementary information, TTPy-H_2O_2 was facilely obtained by a two-step synthetic route. Triphenylamine–thiophene building block containing active aldehyde group was condensed by reacting with 4-methylpyridine in the present of acid to directly afford TTPy which is the product in response of H_2O_2. Then *p*-pinacolborylbenzyl moiety was incorporated into TTPy to get purified TTPy-H_2O_2 as deep red powder by recrystallization and filtration without complicated column chromatography. The structures of the desired products have been confirmed by NMR spectra (Fig. S1-S2 and S4-S5) and HRMS (Fig. S3 and S6).

Studies on optical properties and selective response of H_2O_2

First of all, we investigated the optical properties of TTPy-H_2O_2 to confirm the AIE characteristics and feasibility of imaging by dual channels. The UV-Vis and fluorescence spectra were explored and showed large Stokes shift of TTPy-H_2O_2 (180 nm) and TTPy (180 nm). Exactly separated excitation and emission channels were expected to be adopted in the further imaging in living cells (Fig. 1a and 1b). As designed, TTPy-H_2O_2 presented negligible fluorescence when molecularly dispersed in the solution with low quantum yield (QY_{soln} = 0.8%), and showed remarkable red/NIR emission (670 nm) in the aggregated or solid state (QY_{solid} = 2.4%) (Table S1). The fluorescence intensity was constantly monitored with increasing volume fraction of toluene in DMSO/Toluene solution system. Aggregation-induced fluorescence enhancement was revealed when the fraction of toluene was more than 80% (Fig. 1c and 1d). All these excellent optical properties will be conducive to the detection of H_2O_2 by fluorescence imaging.

Before the practice in living system, we carried out simulated reaction with H_2O_2 in the bottles to investigate the selectivity, reactivity and sensitivity of the presented AIE probe. The fluorescence intensity of TTPy-H_2O_2 (10 μM) reacted with H_2O_2 (100 μM) at different pH values (2–12) was measured. Almost no increase of fluorescence intensity was observed at low pH value, while sudden enhancement took place when the pH value was higher than 6.0 and the fluorescence intensity reached a plateau at about 10.0 (Fig. 1e). This phenomenon implicated that mild alkaline condition may be in favour of this reaction. TTPy-H_2O_2 also showed good stability in various pH values with unchanged fluorescence intensity.[1, 2] After various considerations of reaction efficiency and physiological environment, we chose pH value of 7.4 in the DMSO/PBS buffer (3:7 v/v) as the standard reaction condition.

In order to confirm the selectivity, TTPy-H_2O_2 was incubated with active molecules in the living system respectively, including ROS (OCl^-, $O_2^{\cdot-}$, TBHP and ·OH), reactive nitrogen species (NO), reductive species (GSH, Vc), amino acids (Cys, Glu and Arg) and vital metal ions (Fe^{3+}, Ca^{2+} and Mg^{2+}). As shown in Fig. 1f, all the fluorescence intensity displayed negligible change except H_2O_2 which showed a remarkable 37.5-fold enhancement. This result provided powerful support for the selective monitoring of H_2O_2 in living cells without interference by other active molecules (Fig. 1f).

Afterwards, the response time of TTPy-H_2O_2 (10 μM) in the presence or absence of H_2O_2 (100 μM) was studied. As displayed in Fig. 1f and 1g, there was almost no change of emission in the absence of H_2O_2, suggesting that the excellent stability of TTPy-H_2O_2 under the detection condition. Conversely, after adding H_2O_2, the fluorescence intensity at 590 nm was rapidly increased at the beginning and gradually reached the plateau around 50 minutes. The monitoring by liquid chromatography-mass spectrometry further elucidated that TTPy was generated from TTPy-H_2O_2. The titration experiment was conducted with different concentration of H_2O_2. The fluorescence intensity and the plot of peak intensity at 590 nm versus related concentration were exhibited in Fig. 1g and 1h. A linear relationship in the range of 0 to 30 μM was illustrated with the square of correlation coefficient equalling to 0.98. Besides, the detection limit (LOD) of TTPy-H_2O_2 towards H_2O_2 was estimated to be 0.25 μM in terms of $3\sigma/B$ formula (σ is the standard deviation of blank measurements, n = 11, and B is the slope of the linear equation). Finally, the peak intensity reached a plateau at a concentration of 80 μM which indicated the saturated concentration of this reaction (Fig. 1i and 1j). Above experimental

results testified that TTPy-H_2O_2 was an excellent AIE bioprobe for the selective and sensitive detection of H_2O_2, by displaying the significant fluorescence change.

Studies on capacity of ROS generation upon light irradiation

For the purpose of killing of cancer cells by PDT, the capacity of TTPy-H_2O_2 to generate ROS upon light irradiation was studied by utilizing two different indicators. The increase of fluorescence intensity of dichlorofluorescin (DCFH) commonly indicated that the total content of all kinds of ROS, while the decrease of fluorescence intensity of 9,10-anthracenediyl-bis (methylene)-dimalonic acid (ABDA) specifically indicated the content of singlet oxygen ($^1O_2$) (Fig. 1k and 1l). Hence, rapid and considerable change in fluorescence intensity of DCFH and absorption intensity of ABDA suggested that TTPy-H_2O_2 can efficiently generate ROS containing various species upon white light irradiation. While the capacity of TTPy was slightly weaker to generate ROS mainly containing $^1O_2$. It was reasonable due to the weaker D–A interaction of TTPy.

Investigation on the organelle targeting ability of TTPy-H_2O_2 before and after responding to H_2O_2

Encouraged by above encouraging results, we made attempts to apply for the real-time detection of H_2O_2 in living cells. We investigated the organelle targeting ability of TTPy-H_2O_2 before and after responding to H_2O_2 using CLSM. Importantly, two separated imaging channels were screened for respectively monitoring the fluorescence in cells before and after responding to H_2O_2. The red channel for TTPy-H_2O_2 was used at the emission wavelength range from 650 nm to 700 nm (λ_{ex} = 488 nm), meanwhile, the yellow channel for TTPy was used at the emission wavelength range from 410 nm to 550 nm (λ_{ex} = 405 nm). The red fluorescence was clearly shown by incubating TTPy-H_2O_2 (5 μM) with HeLa cells for 30 min, which was well merged with the commercial MitoTracker Deep Red with a Person's colocalization coefficient of 0.89 (Fig. 2a). No fluorescence was observed in yellow channel. The colocalization study in HepG2 cells and Lo2 cells further confirmed the results (Fig. S9). After treating H_2O_2 (50 μM) for 1 h, the bright yellow fluorescence was emerged, which shared the good overlap with commercial lipid droplet (LD) Tracker Deep Red (Person's colocalization coefficient of 0.91) (Fig. 2b). These interestingly phenomena elucidate that TTPy-H_2O_2 was a mitochondria-targeting probe with red/NIR emission, and could specifically light up LD with bright yellow fluorescence by the selective response to H_2O_2 in living cells. Compared with commercial MitoTracker Green, TTPy-H_2O_2 exhibited better photostability with minor decrease of fluorescence intensity, indicating a good prospect in real-time monitoring (Fig. 2c and S8).

Next, the cell viability was firstly evaluated using MTT assay in multiple cell lines (Fig 2d, S15 and S16). Without light irradiation, both TTPy-H_2O_2 and TTPy exhibited low cytotoxicity towards HeLa cells, HepG2 cells and Lo2 cells. The different concentrations of H_2O_2 were studied to ensure the non-toxic to cells under experimental conditions (Fig. S14). Upon white light irradiation, the cell viability gradually decreased along with increasing concentration of TTPy-H_2O_2 and irradiation time, even as low as 5%. The cell viability of TTPy was slightly higher than those treated by TTPy-H_2O_2, which was in agree with above results

in Fig 1. These results indicated that both of TTPy-H_2O_2 and TTPy were suitable for imaging with good biocompatibility and PDT of cancer cells with efficient ROS generation ability.

Fluorescence imaging of selective detection of H_2O_2 in living cells

In order to explore real-time detection of H_2O_2 in cancer cells, we evaluated the responsiveness of TTPy-H_2O_2 by incubating with different concentration of H_2O_2. The CLSM imaging displayed clear filamentous morphology of the mitochondria with red fluorescence in HeLa cells. LD was already lighted up in the present of low concentration of H_2O_2 (25 μM), and became brighter along with increasing concentration (Fig. S10). When H_2O_2 (50 μM) was added, the fluorescence intensity in yellow channel was observed to gradually enhance at the different time points, and that in red channel decreased (Fig. 3). More and more LD were visualized. All these results suggested that TTPy was firstly produced around mitochondria by the reaction between TTPy-H_2O_2 and H_2O_2, and might undergo entering into the LDs owing to its hydrophobic property.

The imaging with collaborative changes of fluorescence and targeting organelle was also examined by endogenous H_2O_2. It was proven that phorbol myristate acetate (PMA) can stimulate cells to produce H_2O_2.[43] Hence, we incubated HeLa cells with TTPy-H_2O_2 (5 μM) for 30 min. Then PMA (2 μg/mL) was added to test the response of TTPy-H_2O_2 to endogenous H_2O_2. The yellow fluorescence was clearly visualized in LD after 90 min of incubation, indicating that TTPy-H_2O_2 can sensitively respond to not only exogenous but also endogenous H_2O_2 in living cells (Fig. 4).

Intracellular ROS detection and PDT of cancer cells

With the explicit indications of the changes in fluorescence and targeting organelle, cancer cells were expected to be identified by our AIE probe, TTPy-H_2O_2. Afterwards, intracellular ROS generation ability of TTPy-H_2O_2 was investigated in HeLa cells utilizing 2′,7′-dichlorodi-hydrofluorescein diacetrate (DCFH-DA) as a ROS fluorescence indicator. In the experiment, H_2O_2 was removed after incubating with TTPy-H_2O_2 for 1 h in HeLa cells. And DCFH-DA was added for imaging the intracellular ROS which were generated by both TTPy-H_2O_2 in the mitochondria and TTPy in the LD. This PDT strategy combining ROS-induced damages in two vital organelles was expected to be more efficient in killing the cancer cells. The CLSM of cells showed obvious green fluorescence upon 5 sec laser irradiation, and the fluorescence was enhanced sharply along with increased irradiation time (Fig. S13). After laser irradiation for 100 sec, ROS-induced cell morphological changes including the destruction of cytoskeleton and the leaking of cytosol were indicated by the fluorescence of DCFH-DA, while the control cells without TTPy-H_2O_2 staining showed almost no change (Fig. S12). More interestingly, the red fluorescence of TTPy-H_2O_2 maintained superb photostability, which can monitor the morphological change of mitochondria from intact filamentous structure to fragmented and fuzzy form during the irradiation period.[44] The imaging in yellow channel of TTPy also indicated the growing level of H_2O_2 (Fig. 5a and 5b). All above messages suggested the outstanding performance of TTPy-H_2O_2 in ROS generation in living cells.

Moreover, live/dead cell staining assay was carried out to evaluate the PDT effect by using Calcein-AM (green colour for live cells)/propidium iodide (PI) (red colour for dead cells) staining. HeLa cells was incubated with TTPy-H_2O_2 (5 μM) for 30 min,

followed the treatment by 50 μM H_2O_2 for 1 h. The cells treated with (serve as experimental group) or without (serve as control group) light irradiation (20 min) were further cultured for 2 h. The CLSM imaging was conducted after Calcein-AM/PI staining for 30 min. As shown in Fig. 5c and 5d, strong green fluorescence of Calcein-AM was visible in the control group, indicating the good biocompatibility of TTPy-H_2O_2 and TTPy. Oppositely, bright red fluorescence of PI was detected in the experimental group, illustrating the marvelous effect of our strategy for controllable photoablation of cancer cells (Fig. S17). Overall, after responding to H_2O_2, this system was successfully showed PDT effects on the cancer cells.

Conclusions

In summary, TTPy-H_2O_2, as a versatile mitochondria-targeting probe, has been utilized for selective monitoring of H_2O_2 in living cells and PDT-induced ablation of cancer cells. This probe was constructed by elaborate molecular design and simple synthetic method, possessing distinct superiorities of aggregation-induced red/NIR emission, large Stokes-shift, good biocompatibility, and prominent ROS generation ability upon light irradiation. The red fluorescence of TTPy-H_2O_2 in mitochondria was observed to become bright yellow fluorescence which can specifically light up LD in living cells. This novel collaborative imaging of both mitochondria and LD has been applied for the efficient photodynamic therapy on cancer cells. Besides, the remarkable photostability of TTPy-H_2O_2 enabled real-time monitoring of the morphological change of mitochondria in the process of PDT. This interesting strategy will provide a novel insight for developing real-time detection systems towards bioactive molecules in assistance of "always-on" AIE bioprobes.

Conflicts of interest

There are no conflicts to declare.

Acknowledgements

This work was partially supported by the Natural Science Foundation of China (21907068), the China Postdoctoral Science Foundation Grant (2019M653003). Science and Technology Plan of Shenzhen (JCYJ20200109110608167)

Notes and references

1 B. C. Dickinson and C. J. Chang, *Nat. Chem. Biol.,* 2011, **7**, 504-511.

2 P. D. Ray, B. W. Huang and Y. Tsuji, *Cell. Signal.,* 2012, **24**, 981-990.

3 P. H. G. M. Willems, R. Rossignol, C. E. J. Dieteren, M. P. Murphy and W. J. H. Koopman, *Cell Metab.,* 2015, **22**, 207-218.

4 M. D. Brand, *Free Radical Bio. Med.,* 2016, **100**, 14-31.

5 H. Sies, *Redox Biol.,* 2017, **11**, 613-619.

6 J. M. Roscoe and C. S. Sevier, *Cells* 2020, **9**, 2314.

7 T. P. Szatrowski and C. F. Nathan, *Cancer Res.,* 1991, **51**, 794-798.

8 C. Behl, J. B. Davis, R. Lesley and D. Schubert, *Cell* 1994, **77**, 817-827.

9 M. T. Lin and M. F. Beal, *Nature* 2006, **443**, 787-795.

10 M. Giorgio, M. Trinei, E. Migliaccio and P. G. Pelicci, *Nat. Rev. Mol. Cell Bio.,* 2007, **8**, 722-728.

11 P. I. Moreira, C. Carvalho, X. Zhu, M. A. Smith and G. Perry, *BBA – Mol. Basis Dis.,* 2010, **1802**, 2-10.

12 J. R. Stone, *Arch. Biochem. Biophys.,* 2004, **422**, 119-124.

13 M. Lopez-Lazaro, *Cancer Lett.,* 2007, **252**, 1-8.

14 H. Hagen, P. Marzenell, E. Jentzsch, F. Wenz, M. R. Veldwijk and A. Mokhir, *J. Med. Chem.,* 2012, **55**, 924-934.

15 B. C. Dickinson, C. Huynh and C. J. Chang, *J. Am. Chem. Soc.,* 2010, **132**, 5906-5915.

16 A. R. Lippert, G. C. V. De Bittner and C. J. Chang, *Acc. Chem. Res.,* 2011, **44**, 793-804.

17 X. Chen, X. Tian, I. Shin and J. Yoon, *Chem. Soc. Rev.,* 2011, **40**, 4783-4804.

18 J. Chan, S. C. Dodani and C. J. Chang, *Nat. Chem.,* 2012, **4**, 973-984.

19 J. Xu, Y. Zhang, H. Yu, X. Gao and S. Shao, *Anal. Chem.,* 2016, **88**, 1455-1461.

20 Z. Wu, M. Liu, Z. Liu and Y. Tian, *J. Am. Chem. Soc.,* 2020, **142**, 7532-7541.

21 G. Yang, Z. Liu, R. Zhang, X. Tian, J. Chen, G. Han, B. Liu, X. Han, Y. Fu, Z. Hu and Z. Zhang, *Angew. Chem. Int. Ed.,* 2020, **59**, 16154-16160.

22 J. Luo, Z. Xie, J. W. Y. Lam, L. Cheng, H. Chen, C. Qiu, H. S. Kwok, X. Zhan, Y. Liu, D. Zhu and B. Z. Tang, *Chem. Commun.,* 2001, 1740-1741.

23 N. Song, Z. Zhang, P. Liu, Y.-W. Yang, L. Wang, D. Wang and B. Z. Tang, *Adv. Mater.*, 2020, **32**, 2004208.

24 T. Han, D. Yan, Q. Wu, N. Song, H. Zhang and D. Wang, *Chin. J. Chem.*, 2020, **38**, DOI: 10.1002/cjoc.202000520.

25 W. Xu, D. Wang and B. Z. Tang, *Angew. Chem. Int. Ed.*, 2020, **59**, DOI: 10.1002/anie.202005899.

26 Z. Zhang, W. Xu, M. Kang, H. Wen, H. Guo, P. Zhang, L. Xi, K. Li, L. Wang, D. Wang and B. Z. Tang, *Adv. Mater.*, 2020, **32**, 2003210.

27 M. Kang, Z. Zhang, N. Song, M. Li, P. Sun, X. Chen, D. Wang and B. Z. Tang, *Aggregate*, 2020, **1**, 80-106.

28 W. Xu, D. Wang and B. Z. Tang, *Angew. Chem. Int. Ed.*, 2020, **59**, DOI: 10.1002/anie.202005899.

29 W. Zhang, W. Liu, P. Li, F. Huang, H. Wang and B. Tang, *Anal. Chem.,* 2015, **87**, 9825-9828.

30 Z. Song, R. T. Kwok, D. Ding, H. Nie, J. W. Lam, B. Liu and B. Z. Tang, *Chem. Commun.,* 2016, **52**, 10076-10079.

31 Y. Liu, J. Nie, J. Niu, F. Meng and W. Lin, *Sci. Rep.,* 2017, **7**, 7293.

32 X. Wang, Y. Huang, W. Lv, C. Li, W. Zeng, Y. Zhang and X. Feng, *Anal. Meth.,* 2017, **9**, 1872-1875.

33 G. Jiang, C. Li, X. Liu, Q. Chen, X. Li, X. Gu, P. Zhang, Q. Lai and J. Wang, *Adv. Opt. Mater.,* 2020, **8**, 2001119.

34 N. Yang, W. Xiao, X. Song, W. Wang and X. Dong, *Nano-Micro Lett.,* 2020, **12**, DOI: 10.1007/s40820-019-0347-0.

35 L. C. Lo and C. Y. Chu, *Chem. Commun.,* 2003, 2728-2729.

36 H. Zhu, J. Fan, J. Du and X. Peng, *Acc. Chem. Res.,* 2016, **49**, 2115-2126.

37 W. Xu, M. M. S. Lee, J.-J. Nie, Z. Zhang, R. T. K. Kwok, J. W. Y. Lam, F.-J. Xu, D. Wang and B. Z. Tang, *Angew. Chem. Int. Ed.*, 2020, **59**, 9610-9616.

38 D. Wang, H. Su, R. T. K. Kwok, X. Hu, H. Zou, Q. Luo, Michelle M. S. Lee, W. Xu, J. W. Y. Lam and B. Z. Tang, *Chem. Sci.,* 2018, **9**, 3685-3693.

39 D. Wang, M. M. S. Lee, G. Shan, R. T. K. Kwok, J. W. Y. Lam, H. Su, Y. Cai and B. Z. Tang, *Adv. Mater.,* 2018, **30**, 1802105.

40 Y.-Y. Huang, P. Mroz, T. Zhiyentayev, S. K. Sharma, T. Balasubramanian, C. Ruzie, M. Krayer, D. Fan, K. E. Borbas, E. Yang, H. L. Kee, C. Kirmaier, J. R. Diers, D. F. Bocian, D. Holten, J. S. Lindsey and M. R. Hamblin, *J. Med. Chem.,* 2010, **53**, 4018-4027.

41 S. Xu, Y. Duan and B. Liu, *Adv. Mater.,* 2020, **32**, 1903530.

42 G. Feng, G.-Q. Zhang and D. Ding, *Chem. Soc. Rev.,* 2020, **49**, 8179-8234.

43 E. Gallin and S. Green, *Blood* 1987, **70**, 694-701.

44 S. Grandemange, S. Herzig and J. C. Martinou, *Semin. Cancer Biol.,* 2009, **19**, 50-56.

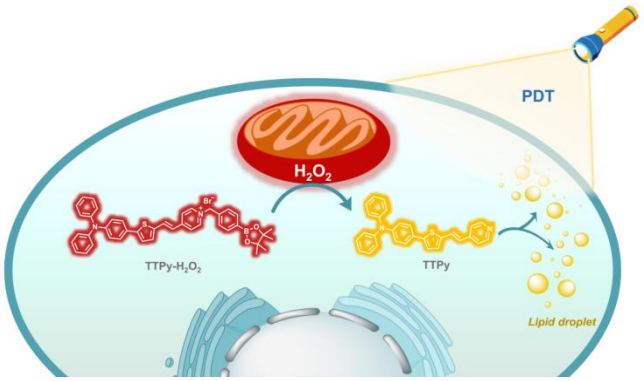

Scheme 1. Schematic illustration of H_2O_2 responsive AIE probe, TTPy-H_2O_2, with selective organelle-targeting for PDT on cancer cells.

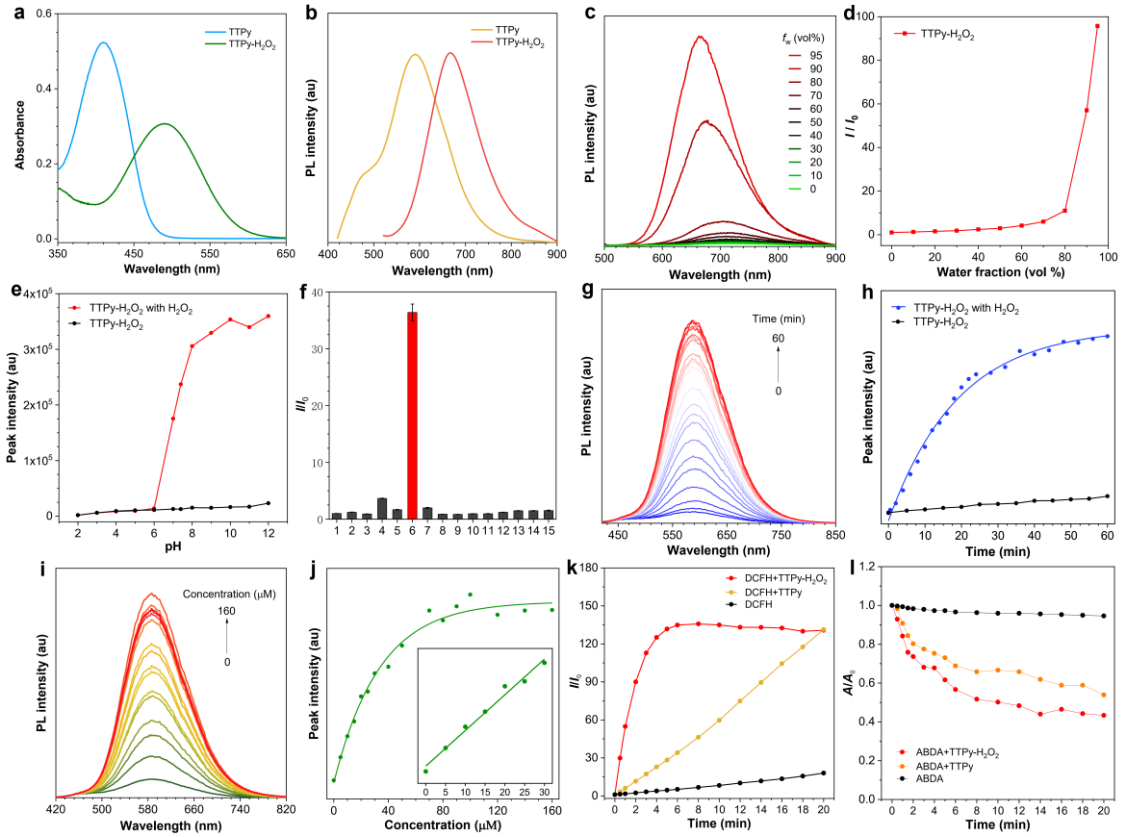

Figure 1. Characterization and H_2O_2 response. Absorption spectra (a) and PL spectra (b) of TTPy-H_2O_2 and TTPy (10 μM) in DMSO/PBS buffer (3:7 v/v, pH 7.4); (c) PL spectra of TTPy-H_2O_2 (10 μM) in DMSO/Toluene mixtures with different toluene fractions (f_w); λ_{ex} = 500 nm; (d) The plot of the relative emission intensity (I/I_0) versus the composition of the toluene mixture of TTPy-H_2O_2; (e) The plot of fluorescence intensity at 590 nm of TTPy-H_2O_2 (10 μM) in DMSO/PBS buffer (3:7 v/v) with different pH values; (f) The selectivity of TTPy-H_2O_2 responses to various analysts. (1: Blank, 2: ClO^-, 3: $O_2^{\cdot-}$, 4: TBHP, 5: ·OH, 6: H_2O_2, 7: NO, 8: Cys, 9: GSH, 10: Vc, 11: Glu, 12: Arg, 13: Fe^{3+}, 14: Ca^{2+}, 15: Mg^{2+}); (g) PL intensity and (h) the plot of peak intensity at 590 nm of TTPy-H_2O_2 (10 μM) in response to H_2O_2 (100 μM) at different time points; (i) PL intensity of TTPy-H_2O_2 (10 μM) in response to H_2O_2 with different concentrations (0-160 μM); (j) The plot of peak intensity at 590 nm of TTPy-H_2O_2 (10 μM) in response to H_2O_2 with different concentrations. Inset: Linear plot of peak intensity against H_2O_2 concentration (0-30 μM); (k) Total ROS generation of TTPy-H_2O_2 and TTPy upon white light irradiation using DCFH as indicator; (l) Singlet oxygen generation of TTPy-H_2O_2 and TTPy upon white light irradiation using ABDA as indicator.

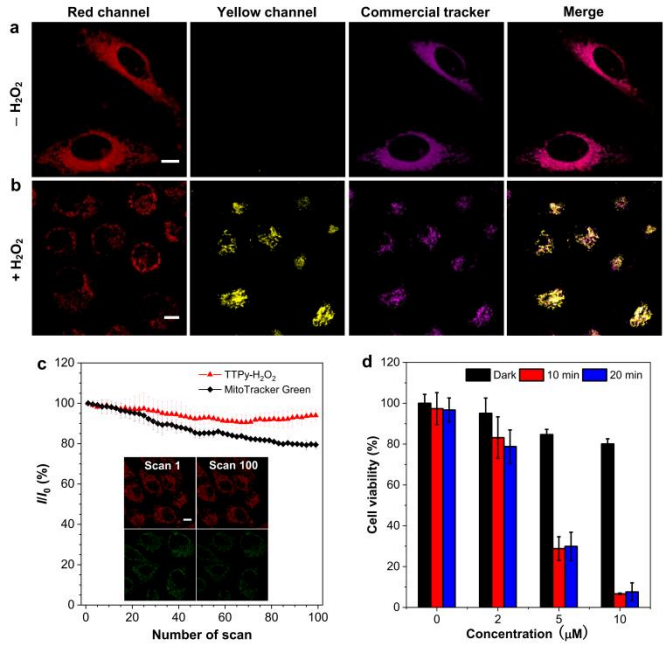

Figure 2. The organelle colocalization and optical properties of TTPy-H_2O_2 before and after the response of H_2O_2 in HeLa cells. (a) Confocal colocalization imaging of TTPy-H_2O_2 (5 μM) with commercial MitoTracker Deep Red (2 μM) incubated without H_2O_2; (b) Confocal colocalization imaging of TTPy-H_2O_2 (5 μM) after incubation with H_2O_2 (50 μM) for 1 hour, then the cells were stained with commercial lipid droplet (LD) Tracker Deep Red (2 μM). Red channel: λ_{ex} = 488 nm, λ_{em} = 650-700 nm; Yellow channel: λ_{ex} = 405 nm, λ_{em} = 410-550 nm; Commercial tracker channel: λ_{ex} = 640 nm, λ_{em} = 650-700 nm. (c) Photostability of TTPy-H_2O_2 and MitoTracker Green. λ_{ex} = 488 nm; Laser power = 0.6 %. (d) Cell viability stained with different concentrations of TTPy-H_2O_2 in the absence or presence of white light irradiation. Scale bar: 10 μm.

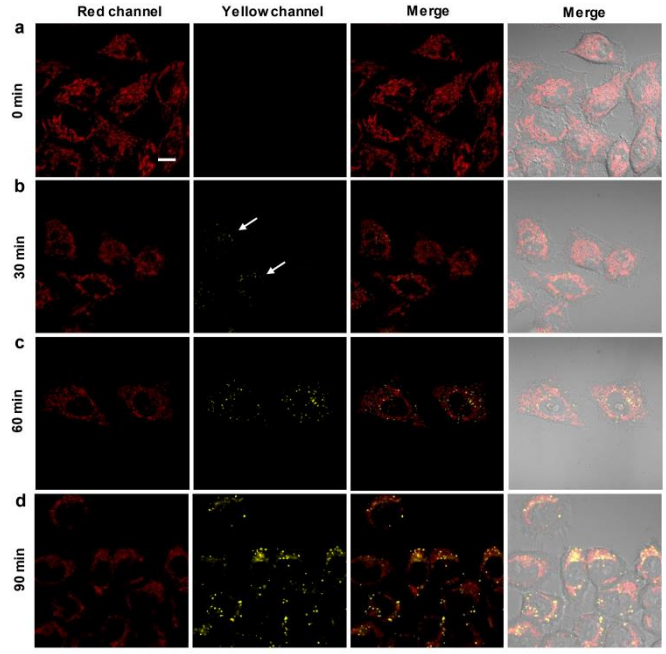

Figure 3. Confocal fluorescence imaging of TTPy-H_2O_2 incubated with H_2O_2 (50 μM) at different time points in HeLa cells. (a) 0 min; (b) 30 min; (c) 60 min and (d) 90 min (white arrows highlighted LD with yellow florescence). Red channel: λ_{ex} = 488 nm, λ_{em} = 650-700 nm; Yellow channel: λ_{ex} = 405 nm, λ_{em} = 410-550 nm; Scale bar: 10 μm.

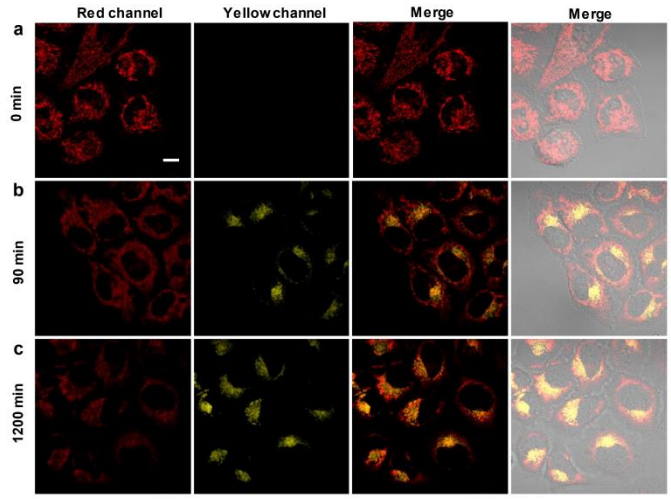

Figure 4. Confocal fluorescence imaging of HeLa cells incubated with TTPy-H_2O_2 for 30 min, followed by the incubation with PMA (2 μg/mL) to produce more endogenous H_2O_2 at different time points. (a) 0 min; (b) 90 min; (c) 120 min. Red channel: λ_{ex} = 488 nm, λ_{em} = 650-700 nm; Yellow channel: λ_{ex} = 405 nm, λ_{em} = 410-550 nm; Scale bar: 10 μm.

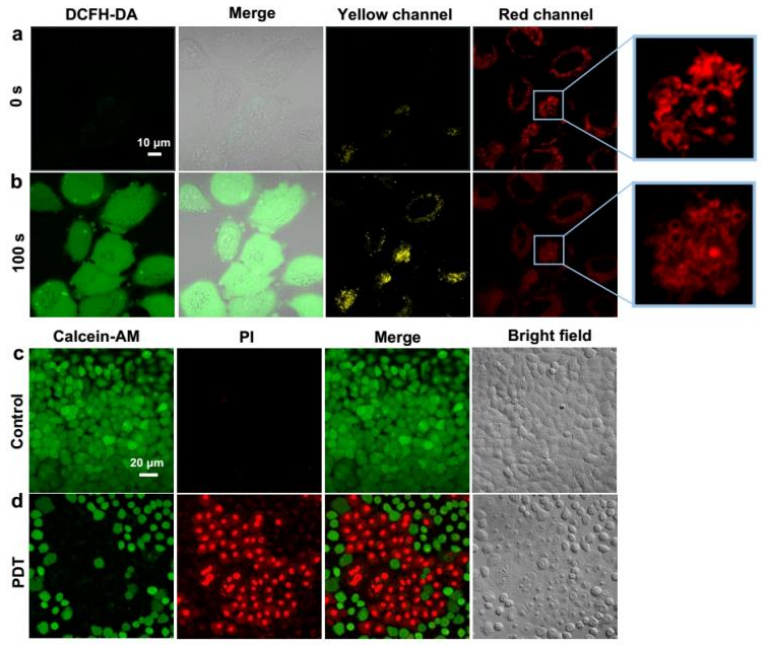

Figure 5. Confocal fluorescence imaging of photodynamic therapy of HeLa cells. (a, b) Intracellular ROS level after incubated with TTPy-H_2O_2 for 30 min, followed by the staining with DCFH-DA (10 μM) upon 488nm laser irradiation. Red channel: λ_{ex} = 488 nm, λ_{em} = 650-700 nm; Yellow channel: λ_{ex} = 405 nm, λ_{em} = 410-550 nm; Scale bar: 10 μm. (c and d) Live/dead cell staining of Calcein-AM/PI after white light irradiation (16 mW/cm^2) for 20 min. Scale bar: 20 μm.